X-ray reflectivity of multilayers with non-continuous interfaces

2002 J. Phys.: Condens. Matter 14 5303

(http://iopscience.iop.org/0953-8984/14/21/305)

INSTITUTE OF PHYSICS PUBLISHING JOURNAL OF PHYSICS: CONDENSED MATTER

J. Phys.: Condens. Matter **14** (2002) 5303–5314 PII: S0953-8984(02)34879-3

X-ray reflectivity of multilayers with non-continuous interfaces

David Rafaja[1,5,6], Hartmut Fuess[1], Daniel Šimek[2], Jiří Kub[2], Josef Zweck[3], Jitka Vacínová[4] and Václav Valvoda[4]

[1] Institute of Materials Science, Darmstadt University of Technology, Petersenstr. 23, D-64287 Darmstadt, Germany
[2] Institute of Physics, Academy of Sciences of Czech Republic, Na Slovance 2, CZ-182 21 Prague, Czech Republic
[3] Institute of Experimental and Applied Physics, University of Regensburg, Universitätsstr. 31, D-93053 Regensburg, Germany
[4] Department of Electronic Structures, Charles University, Ke Karlovu 5, CZ-121 16 Prague, Czech Republic

E-mail: rafaja@tu-darmstadt.de

Received 13 March 2002, in final form 22 April 2002
Published 16 May 2002
Online at stacks.iop.org/JPhysCM/14/5303

Abstract

X-ray specular reflectivity and diffuse scattering calculated using the traditional multilayer model, which assumes continuous, non-intersecting interfaces, are capable of fitting the experimental data obtained on multilayers with non-continuous interfaces. However, wrong refined electron densities and interface roughness are the consequence of an inappropriate structure model. A modification of the Parratt optical formalism combined with the application of the distorted-wave Born approximation was suggested for evaluation of the small-angle x-ray scattering in multilayers with non-continuous interfaces. The influence of the multilayer discontinuity on the small-angle x-ray scattering is characterized by modified Fresnel reflection and transmission coefficients of individual interfaces and by changes in the optical paths in individual layers. The suggested theoretical approach is illustrated on Fe/Au multilayers. Parameters of the structure model obtained from the small-angle x-ray scattering were verified by comparison with results of transmission electron microscopy.

1. Introduction

Periodic multilayers have been studied intensively during the last two decades, especially due to their interesting physical properties. A particular topic are the magnetic multilayers,

[5] Author to whom any correspondence should be addressed.
[6] On leave from: The Department of Electronic Structures, Charles University, Ke Karlovu 5, CZ-121 16 Prague, Czech Republic.

which are mainly investigated because of the giant magnetoresistance (GMR) effect [1] and its applications [2]. Upon investigation of the real structure of periodic multilayers, the small-angle x-ray scattering is employed as a powerful technique. Its advantages are easy preparation of samples for measurement and the non-destructive nature of the method. The small-angle x-ray scattering typically yields information on the index of refraction (that is related to the electron density) and the thickness of individual layers, and on the morphology of interfaces. Usually, the individual layers in a multilayer system are expected to grow as stratified media with continuous interfaces, which do not intersect each other. Thus, the Parratt optical formalism [3–6] combined with the distorted-wave Born approximation (DWBA) [7,8] is typically applied for evaluation of the reflectivity curves [9,10]. However, the GMR effect was found also in highly disturbed metallic multilayers, in which precipitates rather than continuous stratified media develop [11–18]. In particular cases, it was proven experimentally that the GMR effect is more pronounced in multilayers with non-continuous interfaces than in multilayers with rough continuous interfaces. This phenomenon has not been completely explained yet from the theoretical point of view. Some authors associate the increase of GMR with 'sharpening' of diffuse interfaces due to the out-diffusion of elements in systems with limited mutual solubility [19]. Other authors consider breaking up of the magnetic layers due to the grain boundary diffusion and formation of a discontinuous magnetic layer with granular structure [20,21].

For evaluation of the reflectivity curves measured on multilayers with non-continuous interfaces, we suggest a modification of the well established approaches (the Parratt optical formalism [3–6] and the DWBA theory [8,9]). The non-continuous interfaces are assumed to influence the amplitude of the penetrating wave in individual media. It is shown that the calculation based on the traditional model, which assumes continuous interfaces, can still be applied to fit both the coherent and the non-coherent parts of the small-angle x-ray scattering measured on multilayers with non-continuous interfaces. However, the refined parameters of the traditional structure model are wrong as a rule. The effect of the non-continuous interfaces on the shape of the reflectivity curves is illustrated on few simulations and experimental examples of the Fe/Au multilayers. The Fe/Au system is an example of a binary system having a wide miscibility gap at low temperatures. The solubility of gold in iron is less than 2 at.% below 600 °C. The solubility of iron in gold is larger—it is approximately 30 at.% at 600 °C, but it decreases with decreasing temperature [22]. There are no intermediate phases in the Fe/Au system. Therefore, it was surprising that the relative electron density of both species (Fe and Au) must be refined together with the other parameters of the structure model, i.e. the layer thickness and the interface roughness, to arrive at a good match between the experimental and theoretical reflectivity curves.

2. Model of a multilayer with non-continuous interfaces

The structure model of a multilayer with non-continuous interfaces consists of blocks of one atomic species embedded in a matrix of the second atomic species (figure 1(a)). The positions of the blocks match with the positions of original layers in a virtual multilayer. Another interpretation of the model is that the even layers are occasionally short-circuited by bridges of the same material. Horizontal edges of the blocks reflect, whereas their vertical edges form a sufficiently high angle with the surface to render the Fresnel reflection coefficients of the vertical interfaces negligible. Consequently, a high reflectivity of such a disturbed multilayer is anticipated in the specular direction, being more intense than the amount of diffuse scattering. If the blocks become small and if they turn to precipitates with non-reflecting horizontal boundaries, the diffuse scattering becomes dominant and the scattering

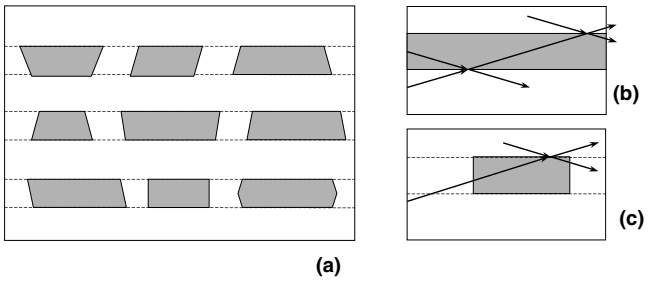

Figure 1. Model of a multilayer with non-continuous interfaces (a). Dashed lines show positions of virtual (continuous) interfaces. Transmission and refraction of x-rays in multilayers with continuous interfaces (b), and in multilayers with non-continuous interfaces (c).

process can be described within the Born approximation (neglecting the multiple scattering) as shown by Rauscher *et al* [23].

Mathematical formulation of the multilayer model with non-continuous interfaces depends on the degree of distortion of the originally plane wave scattered in the sample. If we assume that the scattering on blocks has nearly no effect on the coherence of radiation, the scattered wave is capable of multiple scattering. This assumption is fulfilled if the change of propagation direction, caused by refraction of radiation in media having different indices of refraction, is negligible. This is certainly valid for scattering angles far from the total external reflection (TER) region. In the Fe/Au multilayers with gold at the top, the angular difference, due to the refraction of radiation at the Fe/Au and Au/Fe interfaces, makes 800, 320 and 200 arcsec at the angles of incidence of 0.6°, 1° and 1.5°, respectively. The good coherence of scattered radiation must also be guaranteed by an appropriate shape of blocks. In multilayers consisting of large segments with continuous interfaces, the spherical part of the scattered wave is negligible. This follows from the very narrow shape factor of large blocks (see section 4). Within this structure model, the multilayer structure can be divided into two parts:

(a) regions having locally the same ordering of layers as in multilayers with continuous interfaces and
(b) regions with bridges.

In the regions with well developed multilayer structure (figure 1(b)), the amplitudes of the electromagnetic wave in individual media can be calculated recursively using the Parratt optical formalism [3] as usual ([4–6]):

$$A_j^{(1)} = \frac{\langle f_{j-1}^2 \rangle \langle A_{j-1} \rangle + r_{j,j-1}}{\langle f_{j-1}^2 \rangle \langle A_{j-1} \rangle r_{j,j-1} + 1}. \tag{1}$$

However, the averaged phase shift within the jth layer, $\langle f_j \rangle$, must be employed for calculation, as the radiation penetrates through several different regions at small scattering angles:

$$\langle f_j^2 \rangle = c_j f_{(1)j}^2 + (1 - c_j) f_{(2)j}^2. \tag{2}$$

The individual phase shifts $f_{(1)j}$ and $f_{(2)j}$ in (2) are calculated for the respective layer using

$$f_{(k)j} = \exp(\mathrm{i} q_j^{(k)} t_j / 2). \tag{3}$$

t_j are the thicknesses of the layers and q_j the z component of the diffraction vector in medium j.

$$q_j = k_{j,f} - k_{j,i}, \tag{4}$$

where

$$k_{j,f} = \frac{2\pi}{\lambda}\sqrt{n_j^2 - \cos^2\theta_f} \qquad \text{and} \qquad k_{j,i} = -\frac{2\pi}{\lambda}\sqrt{n_j^2 - \cos^2\theta_i} \tag{5}$$

are the z components of the wavevectors of the incoming (i) and the outgoing wave (f), respectively. θ_i is the angle of incidence, θ_f the outgoing angle.

In symmetrical scattering geometry, the relationship between the diffraction vector, the wavelength λ, the refractory index n_j of the respective layer and the scattering angle in vacuum θ is described by

$$q_j^{(k)} = \frac{4\pi}{\lambda}\sqrt{n_{(k)j}^2 - \cos^2\theta}. \tag{6}$$

The Fresnel reflection coefficients in (1) are exponentially attenuated by the interface roughness σ [24]:

$$r_{j,j-1} = \frac{q_j - q_{j-1}}{q_j + q_{j-1}} \exp\left(-q_j q_{j-1}\frac{\sigma_j^2}{2}\right). \tag{7}$$

To take into account the non-continuity of interfaces, the amplitudes A_{j-1} are replaced by averaged amplitudes $\langle A_{j-1}\rangle$ in the recursive formula (1). In regions with bridges (figure 1(c)), the Fresnel reflection coefficient is equal to zero. Thus, the amplitude of the electromagnetic wave is simply given by the amplitude at the previous interface modified by the phase shift in the respective layer (compare with (1)):

$$A_j^{(2)} = \langle f_{j-1}^2\rangle\langle A_{j-1}\rangle. \tag{8}$$

Again, the phase shift must be calculated for the average composition of the layer according to equation (2). Assuming a good coherence of waves, the average amplitude $\langle A_j\rangle$ is equal to the arithmetic mean of scattering amplitudes in particular regions (given by equations (1) and (8)), which is a sum of individual amplitudes weighted according to the discontinuity fraction of the respective layer, c_j:

$$\langle A_j\rangle = A_j^{(1)}c_j + A_j^{(2)}(1 - c_j). \tag{9}$$

The calculation of amplitudes in individual media is performed recursively, starting from the substrate (A_1), and going towards the surface (A_N). It is assumed that no radiation originates from the infinite substrate ($A_0 = 0$). Finally, the total reflectivity of the multilayer is given by the modulus of the amplitude at the sample surface:

$$R = |A_N|^2. \tag{10}$$

3. Effect of the interface discontinuity on the reflectivity curve

In order to explain the relationship between the amplitudes in discontinuous multilayers and the amplitudes obtained for a well developed multilayer with continuous interfaces, we rewrite the formula (9) in a form which is similar to (1):

$$\langle A_j\rangle = \frac{\langle f_j^2\rangle\langle A_{j-1}\rangle + [c_j + (1 - c_j)\langle f_j^2\rangle^2\langle A_{j-1}\rangle^2]r_{j,j-1}}{\langle f_j^2\rangle\langle A_{j-1}\rangle r_{j,j-1} + 1}. \tag{11}$$

It follows from comparison of equations (1) and (11) that the changes in scattered amplitudes, which are caused by the discontinuous interfaces, apparently modify the Fresnel reflection coefficients r_j. Thus, the multilayer discontinuities yield apparently smaller difference in electron densities of neighbouring layers within the classical model. The angular-dependent

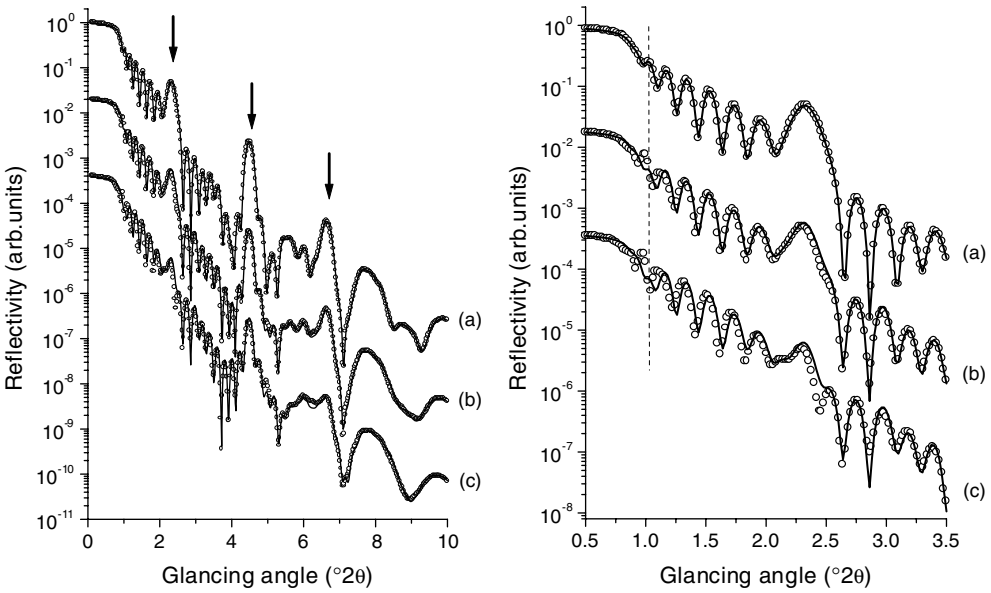

Figure 2. Reflectivity curves calculated for 100% (a), 60% (b) and 30% (c) layer continuity (○) and the respective fit (——). Bragg-like maxima corresponding to the bi-layer thickness are labelled by arrows. The shift of the foremost Kiessig oscillations to lower scattering angles is shown at the right-hand side.

change of the scattering amplitude, which is hidden in the phase shift, is compensated by a change of interface roughness (see equation (7)).

This particular conclusion is illustrated on some numerical examples. The basic multilayer structure, which was used for calculation of the reflectivity curves shown in figure 2, consists of 50 Å gold buffer and the Fe/Au (30/10 Å) × 8 superstructure. The entire multilayer structure is finished by an additional 20 Å of gold on the top as in the experimental cases (section 5). The interface roughness applied for the simulation increased gradually, starting with 3 Å at the buffer and ending with 7 Å at the sample surface. The continuities of interfaces were 100, 60 and 30%. Results of the numerical simulation have shown that the intensity of Bragg-like peaks decreases with increasing discontinuity of interfaces. Another consequence of the interface discontinuity was a shift of the foremost Kiessig oscillations related to the entire multilayer thickness towards smaller scattering angles. This phenomenon cannot be emulated via changes in electron densities of individual layers, as neither the decreasing difference in electron densities nor a high interface roughness can fully substitute the angular-dependent change of the Fresnel reflection coefficient.

To inspect the changes in the parameters of the structure model, which are caused by the presence of non-continuous interfaces, the simulated reflectivity curves were fitted by employing the traditional multilayer model with continuous interfaces. The match between the experimental and theoretical reflectivity curves is very good, except the region just behind the edge of TER, as discussed above. Also the refined thickness of individual layers is well reproduced (table 1), but the refined electron density of gold becomes smaller, whereas the electron density of iron becomes larger in comparison with their values used previously for the reflectivity curve simulation. In addition, the refined interface roughness of all interfaces increased apparently as predicted.

Table 1. An overview of structure parameters, which were obtained for discontinuous multilayers from the reflectivity curve fitting employing the multilayer model with continuous interfaces.

Parameter	Simulation		Refinement		
Layer continuity			100%	60%	30%
Thickness	Fe	30 Å	30.0 Å	30.1 Å	30.2 Å
	Au	10 Å	10.0 Å	9.9 Å	9.9 Å
Rel. electron	Fe	1.00	1.00	0.98–1.17	0.99–1.32
density	Au	1.00	1.00	0.98–0.79	0.97–0.65
Interface	Fe	3–7 Å	3–7 Å	+5%	+11%
roughness	Au	3–7 Å	3–7 Å	+4%	+10%

4. Effect of the interface discontinuity on the diffuse scattering

Theoretical description of the diffuse scattering in multilayers with continuous interfaces is based on the DWBA concept [8, 9]. To describe the diffuse scattering in multilayers with discontinuous interfaces, the same approach was employed as in section 2. The dominant factor influencing the amount of the semi-kinematical diffuse scattering by corrugated layers is the intensity of the wave penetrating into the multilayer, which is usually expressed in terms of Fresnel transmission coefficients:

$$t_{j,j-1} = \frac{2k_j}{k_j + k_{j-1}}, \tag{12}$$

where k is the wavevector of the incoming or the outgoing wave(s). The Fresnel transmission coefficient increases exponentially with increasing interface roughness [24]:

$$t_{j,j-1} = \frac{2k_j}{k_j + k_{j-1}} \exp\left[(k_j - k_{j-1})^2 \frac{\sigma_j^2}{8}\right]. \tag{13}$$

At the non-continuous parts of the interfaces (figure 1(c)), the incoming wave is not reflected ($r_{j,j-1} = 0$), but fully transmitted ($t_{j,j-1} = 1$). Similarly to (9), the average transmission coefficient can be written as

$$\langle t_{j,j-1} \rangle = t^{(1)}_{j,j-1} c_j + t^{(2)}_{j,j-1} \left(1 - c_j\right) \tag{14}$$

with $t^{(1)}_{j,j-1}$ from (12) or (13) and with $t^{(2)}_{j,j-1} = 1$. Equation (14) yields

$$\langle t_{j,j-1} \rangle = \frac{k_j \left(1 + c_j\right) + k_{j-1} \left(1 - c_j\right)}{k_j + k_{j-1}} \tag{15}$$

or including the interface roughness

$$\langle t_{j,j-1} \rangle = \frac{k_{j-1}(1 - c_j) + k_j \left[c_j \left\{2 \exp\left[\frac{\sigma_j^2}{8}(k_j - k_{j-1})^2\right] - 1\right\} + 1\right]}{k_j + k_{j-1}}. \tag{16}$$

The limiting cases yield either the equations (12) and (13) for $c_j = 1$, or $\langle t_{j,j-1} \rangle = 1$ for $c_j = 0$. Transmission coefficients of continuous interfaces are never far from unity. Particularly at the Fe/Au interfaces, the absolute value is ranging between 0.5 and 1.5 for $\theta < 1^\circ$. At higher scattering angles, the transmission coefficients are almost equal to unity. The only exception is the surface, i.e. the interface between the vacuum and the uppermost layer, where the Fresnel transmission coefficient starts at zero and reaches a maximum at the critical angle of the uppermost layer material. This dependence of the Fresnel transmission coefficient on the scattering angle is responsible for the shape of the Yoneda wings [25]. Due to the small range

of the Fresnel transmission coefficients within a multilayer, the variations in the incoherently scattered intensity, which are caused by the non-continuous interfaces, are rather weak (in comparison with the changes in the x-ray reflectivity). Thus, a significant increase of the amount of diffuse scattering is not expected. Visible changes are only anticipated near the Yoneda wings. In non-continuous multilayers, they are weaker and shifted due to the apparent change of the index of refraction or to the apparent change of the relative electron density. Concerning the resonant diffuse scattering [26] in multilayers with non-continuous interfaces, its intensity is still predominantly controlled by vertical correlations of the corrugations at the continuous parts of the multilayer.

Another important factor influencing the diffuse scattering is the shape factor of individual blocks. This is described by the function $\Omega_k(x, y)$, which occurs in the modified structure factor [8, 9]

$$\tilde{F} = \sum_k \int_{S_0} \mathrm{d}x\,\mathrm{d}y\,(\mathrm{e}^{|q_z^t|^2 C_j(x,y)} - 1)\mathrm{e}^{-\mathrm{i}(xq_x+yq_y)}\Omega_k(x, y). \tag{17}$$

The summation in (17) is performed over all blocks, k, which lie within the jth layer. $\Omega_k(x, y)$ is equal to unity at the continuous parts of the multilayer, zero elsewhere. Such a function can be expressed in the form of the Heaviside function Y:

$$\Omega_k(x) = Y[L_k(x - x_k) - (x - x_k)^2], \tag{18}$$

where x_k is the position and L_k the lateral size of the kth block. Substituting the Heaviside function (18) into (17), the modified structure factor looks like a convolution with the average shape function of the blocks (the average is from the sum over all blocks in (17)).

This convolution applies also for the specular scattering. For the modified structure factor including the specular scattering [8]

$$\tilde{F} = \sum_k \int_{S_0} \mathrm{e}^{q_z^2 C(x,y)}\mathrm{e}^{-\mathrm{i}(xq_x+yq_y)}\Omega_k(x, y)\,\mathrm{d}x\,\mathrm{d}y \tag{19}$$

we obtain for a smooth continuous multilayer ($C(x, y) = 0$)

$$\tilde{F} = \int_{S_0} \sum_k \Omega_k(x, y)\mathrm{e}^{-\mathrm{i}(xq_x+yq_y)}\,\mathrm{d}x\,\mathrm{d}y. \tag{20}$$

In this particular case, the modified structure factor takes the form

$$\tilde{F} = \sum_k \frac{\sin[q_x \frac{L_k(x)}{2}]\sin[q_y \frac{L_k(y)}{2}]}{q_x q_y}. \tag{21}$$

If the blocks in a multilayer are large, the shape factor yields a very narrow function, which mainly broadens the specular peak into the non-specular direction. The FWHM of the intensity maximum calculated using (21) is approximately 0.04° (150 arcsec) for $L = 5\,\mu$m. This effect is of the same order of magnitude as the effect of the limited coherence of radiation due to the limited spectral purity of radiation and the limited lateral coherence length [27] in the experimental set-up used (section 5). Thus, the dominant effects in the diffuse scattering will still originate at corrugated but continuous parts of the multilayer.

5. Experimental results

The above structure model was applied to Fe/Au multilayers with different thicknesses of individual layers. The nominal compositions were Fe/Au (13/22 Å) × 20, Fe/Au (26/24 Å) × 10 and Fe/Au (70/21 Å) × 13. Details of the sample preparation (RF

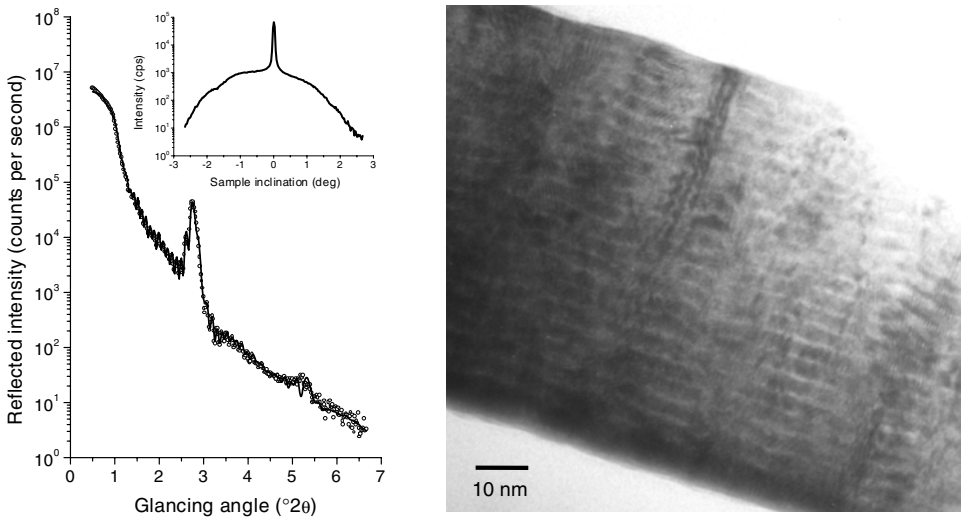

Figure 3. Left: measured (○) and calculated (——) reflectivity curves and the diffuse scattering (sample scan performed at the first Bragg maximum, shown in the inset) of the Fe/Au (13/22 Å) × 20 multilayer deposited on a 60 Å gold buffer. Right: cross-section image of the multilayer as seen by TEM.

diode sputtering) are given in [28] together with the results of the magnetic measurements (magnetization, Kerr rotation). Small-angle x-ray scattering was studied using a double-axis diffractometer (BEDE). As a source of radiation, an 18 kW rotating anode (Rigaku) was used. The radiation of the copper anode was monochromatized by a perfect flat germanium monochromator (reflection 111). A narrow slit having the opening of 70 μm was inserted behind the monochromator. The distance between the anode and the slit was approximately 1 m. Thus, only a part of the Cu Kα_1 arrived at the sample, which allows the primary beam to be regarded as a satisfactory plane wave. The scattered radiation was detected by a scintillation detector. To reduce the amount of diffusely scattered radiation registered by the detector in symmetrical mode, another slit with the width of 80 μm was placed in the front of the detector. The distance between the sample and the second slit was 0.5 m. To estimate the amount of diffuse scattering contributing to the reflectivity curve, off-scans were recorded at the sample inclination of 300 arcsec ($\approx$0.083°) from the symmetrical position. In order to obtain insight into the morphology of interfaces, diffuse scattering was measured via sample scans performed at a constant detector angle.

The first experimental example (figure 3, left) shows the reflectivity curve of the Fe/Au (13/22 Å) × 20 multilayer deposited on a 60 Å gold buffer. The refined thickness of the gold layers was constant through the multilayer stack; the thickness of the iron layers increased gradually from 11 Å at the buffer to 15 Å at the sample surface. The refined interface roughness was 8–9 Å, which is comparable to the thickness of the iron layers. The refined interface continuity was 0.8. The calculation using the traditional multilayer model (with continuous interfaces) yielded the electron density of iron as 1.5 and the electron density of gold as 0.85, which contradict the low mutual solubility of the species at the deposition temperature ($\approx$200 °C). The high amount of resonant diffuse scattering observed in the sample scan performed at the first Bragg maximum indicates a high vertical correlation of the interface roughness. In order to prove the results obtained from x-ray scattering, this multilayer was investigated by transmission electron microscopy. The cross-section image (figure 3,

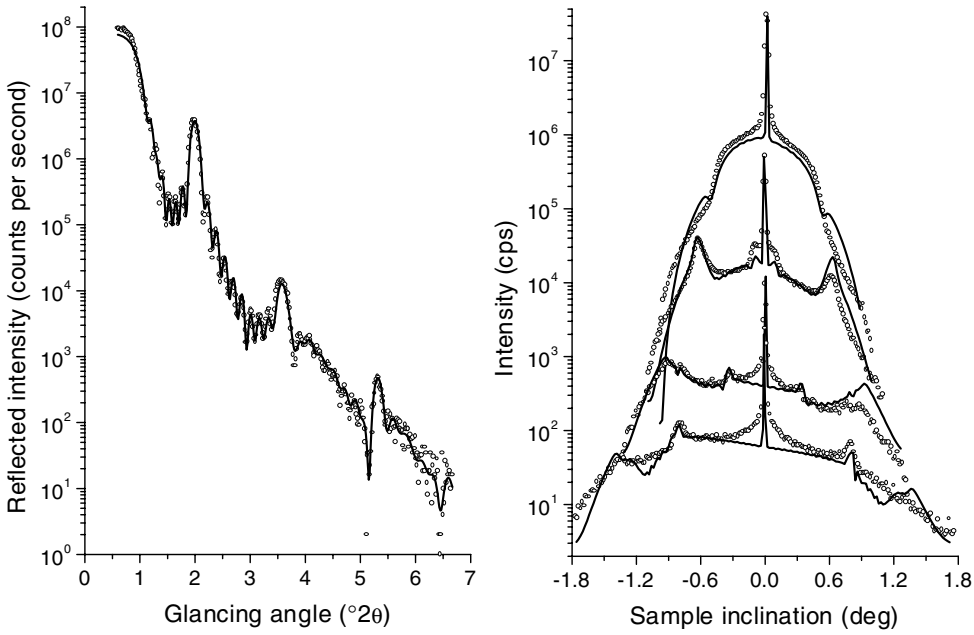

Figure 4. Reflectivity curve (left) and the sample scans (right) measured on the (24/20 Å) × 10 Fe/Au sample. Open circles show the measured intensities; solid curves are used for the fit. The sample scans were taken at the detector angles 2°, 2.22°, 2.67° and 3.56° (from the top to the bottom).

right) showed large regions with well developed multilayer structure. On the other hand, regions were found where the multilayer structure was locally interrupted (by-passed). A direct quantitative comparison of the layer discontinuities obtained from x-ray scattering and from TEM is difficult, as the scope of the two techniques is different. Nevertheless, the two experimental methods yielded principally the same result, showing that the multilayers are partially discontinuous, the amount of discontinuity being of the order of tens of per cent.

The second experimental example (figure 4) shows the small-angle x-ray scattering measured on the (26/24 Å) × 10 Fe/Au sample. The refined layer thicknesses were constant through the multilayer. The refined interface continuity was 90%. The refined interface roughness was 6.5 Å, nearly constant through the multilayer. Evaluation of the sample scans yielded the lateral correlation lengths of 190 Å for gold and 240 Å for iron. The calculation was performed simultaneously for all sample scans using the DWBA theory [26] with modified transmission coefficients (16). The shape factor of the blocks was not taken into account. Therefore, a discrepancy between the experimental data and the fit is evident in the sample scans near the specular peak. The interface roughness was entirely replicated through the multilayer. Thus, the amount of the resonant diffuse scattering is high, as it follows from the intense vertical maxima in the reciprocal space map (figure 5). The dynamical nature of the scattering process was already obvious from the reflectivity curve (figure 4). The reciprocal space mapping confirmed the dynamical effects, as the Bragg-like resonant lines (oblique intensity maxima crossing the Bragg-like peaks) are well developed. On the other hand, the high intensity of the Bragg-like resonant lines is only observed in multilayers with a good periodicity (like in this case). A minor multilayer discontinuity has, in such a case, only negligible effect on the intensity of the Bragg-like resonant lines.

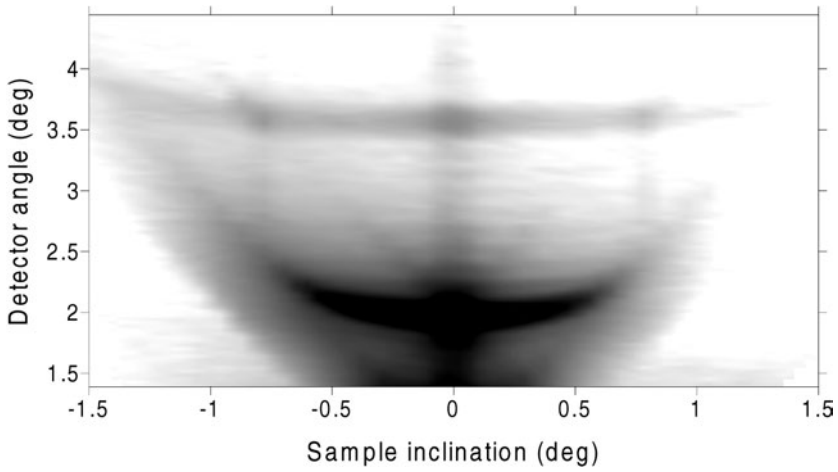

Figure 5. A reciprocal space map of the (24/20 Å) × 10 Fe/Au multilayer.

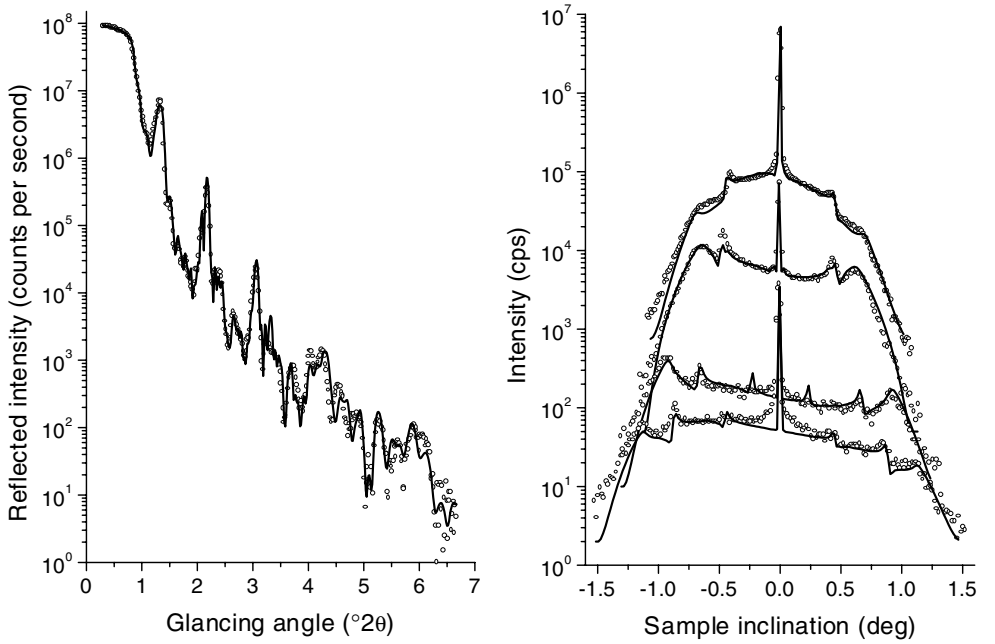

Figure 6. Left: reflectivity curve of the (70/21 Å) × 13 Fe/Au sample deposited on a 280 Å gold buffer. Right: sample scans performed at $2\theta = 2.17^\circ$, 2.30°, 2.65° and 3.07°. Open circles show the measured reflectivity curve, solid curves the best fits.

The above multilayers consisting of thin iron layers were compared with the (70/21 Å) × 13 Fe/Au multilayer deposited on a 280 Å thick gold buffer (figure 6). As the iron layers in the multilayer stack are wide, the non-continuity of interfaces was less probable. This assumption was confirmed by experimental data, as the refined interface continuities and the refined relative electron densities were equal to unity. The interface roughness increased from the buffer (having 8 Å rms roughness) towards the surface, where the rms roughness reached 12 Å. The lateral correlation lengths, calculated from the sample scans, were 180 Å for gold and 380 Å

for iron. The calculated vertical correlation length was 800 Å. In comparison with the previous sample, the calculated sample scan fits the experimental data much better, as the influence of the shape factor on the diffuse scattering is negligible.

6. Discussion

The presented structure model assumes a full coherence of the scattered waves. Thus, it is applicable only to corrugated multilayers, which are broken into reflecting blocks. Nevertheless, it was confirmed by experimental results that reflectivity curves are very sensitive to the interface discontinuities. Therefore, the reflectivity curve fitting can be used to inspect the amount of interface discontinuity. However, the interface discontinuity correlates with the relative electron density and with the interface roughness within the structure model. Thus, this approach yields best results in systems with low mutual solubility.

The amount of incoherent scattering depends, of course, on the size and on the lateral positions of the blocks. The size effect can be understood as a convolution of the modified structure factor calculated for the multilayer with the shape function of the blocks. This holds for both the specular and the non-specular parts of the scattered intensity. However, if the lateral size of the blocks is large, as was the case in presented Fe/Au multilayers, the effect of the interface discontinuity on the diffuse scattering is negligible. The interface discontinuities influence predominantly the specular reflectivity. Consequently, the changes in the reflectivity curve, which lead to the observed variations in the refined electron densities (indices of refraction) are the dominant phenomena, which can be recognized experimentally.

7. Conclusions

A structure model for multilayers with non-continuous interfaces was proposed. Multilayers with partly discontinuous interfaces were described by a model of blocks embedded in a matrix. Calculation of the small-angle x-ray scattering was based on the Parratt optical formalism and on the DWBA theory. It was concluded that the discontinuities of interfaces modify the Fresnel reflection and transmission coefficients and the optical path in the by-passed regions. The structure model was successfully applied to fit reflectivity curves taken on Fe/Au multilayers. Results of the small-angle x-ray scattering were compared with results obtained using transmission electron microscopy.

Numerical simulations of reflectivity curves combined with the back-refinement of parameters of the structure model have shown that the traditional model, which assumes continuous non-intersecting interfaces, is capable of fitting the reflectivity curves measured on multilayers with non-continuous interfaces. However, the interface discontinuities cause apparent changes in the refined electron densities and in the refined interface roughness.

Acknowledgment

DR appreciates the support of this work through the Alexander von Humboldt Fellowship.

References

[1] Baibich M N, Broto J M, Fert A, Nguyen van Dau F, Petroff F, Ethienne P, Creuzet G, Friedrich A and Chazelas J 1988 *Phys. Rev. Lett.* **61** 2472
[2] Daughton J M 1999 *J. Magn. Magn. Mater.* **192** 334
[3] Parratt L G 1954 *Phys. Rev.* **95** 359

[4] Underwood J H and Barbee T W 1981 *Appl. Opt.* **20** 3027
[5] Lee P 1983 *Appl. Opt.* **22** 1241
[6] Vidal B and Vincent P 1984 *Appl. Opt.* **23** 1794
[7] Vineyard G H 1982 *Phys. Rev.* B **26** 4146
[8] Sinha S K, Sirota E B, Garoff S and Stanley H B 1988 *Phys. Rev.* B **38** 2297
[9] Holý V, Kuběna J, Ohlídal I, Lischka K and Plotz W 1993 *Phys. Rev.* B **47** 15 896
[10] Baumbach T, Tixier S, Pietsch U and Holý V 1995 *Phys. Rev.* B **51** 16 848
[11] Iijima M, Shimizu Y, Kojima N, Tanaka A and Kobayashi K 1996 *J. Appl. Phys.* **79** 5602
[12] Jarratt J D and Barnard J A 1996 *J. Appl. Phys.* **79** 5606
[13] Luby Š, Majková E, Špásová M, Jergel M, Senderák R, D'Anna E, Luches A, Martino M, Brunel M and Dmitrenko I M 1998 *Thin Solid Films* **312** 15
[14] Zhou S M *et al* 1998 *J. Appl. Phys.* **83** 900
[15] Mendes J A, de Azevedo M M P, Rogalski M S and Sousa J B 1999 *J. Mater. Process. Technol.* **93** 534
[16] Adam E, Lancon F and Rodmacq B 1999 *Comput. Phys. Commun.* **122** 545
[17] Binns C, Edmonds K W, Baker S H, Maher M J, Thornton S C and Upward M D 2001 *Scr. Mater.* **44** 1303
[18] Öksüzoglu R M, Elmali A, Weirich T E, Fuess H and Hahn H 2000 *J. Phys.: Condens. Matter* **12** 9237
[19] Shelp L F, Tosin G, Carara M, Baibich M N, Gomes A and Schmidt J E 1992 *Appl. Phys. Lett.* **61** 1858
[20] Berkowitz A E, Mitchell J R, Carey M J, Young A P, Zhang S, Spada F E, Parker F T, Hutten A and Thomas G 1992 *Phys. Rev. Lett.* **68** 3745
[21] Dykes J W, Kim Y K, Tsoukatos A, Gupta S and Sanders S C 1996 *J. Appl. Phys.* **79** 5584
[22] Massalski T B, Subramanian P R, Okamoto H and Kacprzak L 1990 *Binary Alloy Phase Diagrams* 2nd edn (Materials Park, Ohio: ASM International)
[23] Rauscher M, Salditt T and Spohn H 1995 *Phys. Rev.* B **52** 16 855
[24] Névot L and Croce P 1980 *Rev. Phys. Appl.* **15** 761
[25] Yoneda Y 1963 *Phys. Rev.* **131** 2010
[26] Holý V and Baumbach T 1994 *Phys. Rev.* B **49** 10 668
[27] Holý V, Pietsch U and Baumbach T 1999 *High Resolution X-Ray Scattering from Thin Layers and Multilayers (Springer Tracts in Modern Physics vol 149)* (Berlin: Springer) p 28
[28] Krishnan R, Das A and Porte M 1997 *J. Magn. Magn. Mater.* **168** 15